Green synthesis of CeO_2 nanoparticles using *Hybanthus enneaspermus* and their cytotoxic effects against human Breast cancer cell line (MCF-7)

[1*]Murugan M. and [2]Kamaraj M.
[1]Department of Biotechnology, Salem Sowdeswari College -636010, Tamil Nadu, India.
[2]Department of Botany, Jamal Mohamed College(Autonomous), Tituchirapalli-620020 Tamil Nadu, India.

Abstract

Biosynthesis of nanoparticles was an important area in the field of nanotechnology which has economic and eco-friendly over chemical and physical methods of synthesis. In present work, synthesis of CeO_2 nanoparticles was achieved using 1 mM Cerium (III) nitrate hexahydrate ($Ce(NO_3)_3$. $6H_2O$ through the extract of *Hybanthus enneaspermus (H. enneaspermus)* as reducing as well as capping agent. Green synthesis of CeO_2 NPs retained the cubic phase which was confirmed by X-ray diffraction studies. TEM images showed that the NPs possessed spherical shape and average particle size of 20-30 nm. EDAX studies determined the elemental compositions were identified for Cerium and oxygen. The FT-IR spectra confirmed the Ce-O stretching bands at 457 cm^{-1} for the CeO_2 NPs. The band gap of the CeO_2 NPs was estimated at 2.9 eV from the UV-Vis spectrum. From the photoluminescence measurements, the broad emission composed of six different bands were found. The green synthesized CeO_2 NPs showed dose dependent response against breast cancer MCF-7 cell line (LD_{50}-10 µg/ml).

Keywords: Biosynthesis of nanoparticles, CeO_2, *Hybanthus enneaspermus*

1. Introduction

Phytosynthesis of metal and metal oxide nanoparticles (NPs) is an emerging field in the nanotechology. Physical and chemical properties conjointly play a vital role in physical, chemical, electrical and optical properties of nanomaterials. Cerium oxide (CeO_2) is a semiconductor with wide band gap energy (3.19 eV) and large exciton binding energy. It is used in wide range of applications such as, catalyst, sensor, solid oxide fuel cells, sun screen cosmetics, bioimaging, biotransformation and antibacterial, activity [1-7]. In recent years, there has been increasing attention towards eco-friendly synthesis of metal oxide nanoparticles using plants, this is because though nanoparticles exhibit exceptional electronic, thermal, antimicrobial and anticancer properties compared to bulk particles. The nanoparticles synthesis causes lot of toxic by-products. The green synthesized nanoparticles do not produce any toxic by-products and also have reported to be more stable compared to chemically synthesized ones. Moreover, the rate of synthesis is also much faster [8].

H. enneaspermus Muell, belonging to family Violaceae, is a herb or under shrup distributed in a tropical and subtropical regions of the world. It is an herb, often with woody troches, found in the warmer parts of India. An infusion of the plant extract is given in case of cholera [9]. The plant has been reported to have anti-inflammatory [10], antitussive [11], antiplamodial [12], anticonvulsant, free radical scavenging activity [13], antidiabetic [14] and antibacterial [15]. The plant is reported to contain aurantiamide acetate, isoarborinol, b-sitosterol and teriterpene [16]. In folklore the plant is used in case of pregnant and parturient women, and in case of gonorrhoea and urinary infections. In Literature green synthesis of CeO_2 NPs by plants alovera [8] and Gloriosa superba [17] have been reported. The present investigation, CeO_2 NPs is synthesized by using *H. enneaspermus* leaf extract. We have studied the structural, optical and cytotoxic activities of CeO_2 NPs. To the best of our knowledge, this is the first report on the green synthesis of CeO_2 NPs by using *Hybanthus enneaspermus* leaf extract and their characterization studies

such as XRD, TEM, EDX, FTIR, UV-Vis, Photoluminescence's and cytotoxic activities analyses are carried out.

2. Experimental methods

2.1. Green synthesis of CeO_2 nanoparticles

The collected *H. enneaspermus* leaves were washed thoroughly with distilled water and shade dried for 2-3 weeks. The dried leaves were powdered to fine particles using a mixer grinder. For the preparation of aqueous leaf extract (ALE), 10 g of leaf powder was dissolved in 100 ml of deionized water followed by boiling at 60 ˚C for 10 min. The ALE was allowed to cool, filtered (Whatman No.1 filter paper-0.42 µm) and refrigerated until further use. Meant for CeO_2 nanoparticles synthesis 90 ml of 1 mM Cerium (III) nitrate hexahydrate ($Ce(NO_3)_3$. $6H_2O$ solution was mixed with 10 ml of leaves extract and allow to stand at room temperature until further color change occurs. This solution was stirred constantly at a temperature of 120 ˚C for 4-6 h. A yellow precipitate formed and then it became a yellowish brown in colour on continuous stirring. Further the precipitate was calcined at 700 ˚C for 5 h. Thus, a CeO_2 nanoparticle was obtained.

2.2. Cell Viability Assay

MTT assay was carried out as described previously [18]. *H. enneaspermus* leaf extracts Capped CeO_2 NPs, in the concentration range 1-500 µg/ml concentration of green synthesis of CeO_2 NPs were added to the wells 24 h after seeding of 5 x 10^3 cells $well^{-1}$ in 200 µL of a fresh culture medium. After 24 and 48 h, 20 µL of a MTT solution [5 mg/mL in phosphate-buffered saline (PBS)] was added to each well, and the plates were wrapped with aluminum foil and incubated for 4 h at 37 ˚C. The purple formazan product was dissolved by the addition of 100 µL of DMSO to each well. Spectro-photometrical absorbance of the purple blue formazan dye was measured in a microplate reader at 570 nm (Biorad 680). Cytotoxicity was determined using Graph pad prism 5 software. The percentage inhibition was calculated, from this data, using the formula
= (mean OD of untreated cells (control) – mean OD of treated cells / mean OD of untreated cells) x 100.

2.3. AO/EB Staining

Acridine orange and ethidium bromide staining was performed as described by Spector et al [19]. The cell suspension of each CeO_2 NPs containing $5x10^5$ cells, was treated with 25 µL of AO and EB solution (3.8 µm of AO and 2.5 µM of EB in PBS) and examined in a fluorescent microscope (Ti-Eclipse) using an UV filter (450-490 nm). One hundred cells per sample were counted in tetraplicate for each dose point. Morphological changes were also observed and photographed.

2.4. Characterization

The Green synthesized CeO_2 NPs samples were subjected to XRD analysis. The XRD pattern is recorded using Cu Kα radiation (λ=1.54060 Å) with nickel monochromator in the range of 2θ from 10º to 80º. The morphology of the synthesized CeO_2 was examined using TEM. Samples for TEM analysis were prepared by drop coating the nanoparticles solutions on carbon-coated copper grids at room temperature. The excess nanoparticles solution was removed with filter paper. The copper grid was finally dried at room temperature and was subjected to TEM analysis by the instrument Tecnai F20 model operated at an accelerating voltage of 200 kV. The samples were analyzed by EDAX (model: ULTRA 55). Moreover, Fourier transform infrared spectroscopy (FTIR) analysis was carried out in the range of 400-4000 cm^{-1}(Perkin Elmer). The UV-Vis-NIR spectrum recorded in the wavelength range 190-1110nm by using Lambda 35. The photoluminescence (PL) measurement was performed on a Perkin Elmer LS 45 spectrometer in the wavelength range of 340-550 nm.

3. Results and discussion

3.1. X-Ray Diffraction Studies

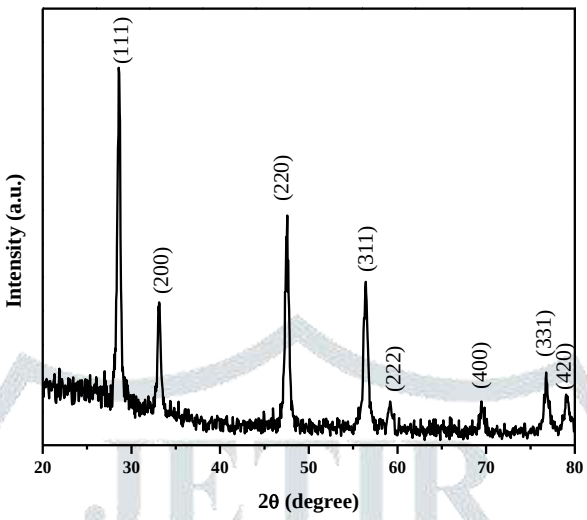

Figure 1: X-ray powder diffraction patterns of CeO_2 NPs using *H.enneaspermus* leaf extract

The X-ray diffraction peaks of CeO_2 NPs synthesized using *Hybanthus enneaspermus* leaf extracts is shown in Fig. 1. The XRD peaks are located at angles (2θ) of 28.563, 33.10 and 47.501 corresponding to (111), (200) and (220) planes of the CeO_2 NPs. Similarly, other peaks found at angles (2θ) of 56.37, 59.13, 69.46, 76.74 and 79.06 are corresponding to (311), (222), (400), (331) and (420) planes of CeO_2 NPs. The standard diffraction peaks show the face-center cubic phase of CeO_2 NPs (JCPDS data card no: 34-0394). The lattice constants 'a' of CeO_2 can be calculated by using the relation.

$$\frac{1}{d^2} = \left(\frac{h^2 + k^2 + l^2}{a^2}\right)$$

The calculated values 'a' is 5.416Å for CeO_2 NPs. The unit cell volume calculated by the above relation is $V = a^3$. The unit cell volumes are found to be 158.867 $Å^3$ for the CeO_2 NPs. The average crystallite size of the samples is calculated after appropriated background corrections from X-ray line broadening of the diffraction peaks using Debye scherrer's formula.

$$\text{Average crystallite size } D = \frac{k\lambda}{\beta_{D\ cos\theta}}$$

Where λ is the wavelength of X-ray used (1.5405Å), β is the angular peak width at half maximum in radians and θ is Bragg's diffraction angle. The average particle size is reduced from 24 nm for CeO_2 NPs respectively.

3.2. Transmission electron microscopy

HRTEM images of CeO_2 nanoparticles (Fig. 2a) reveal spherical shape of the particles with sizes in the range from 20 to 30 nm. The high crystallinity of the powder leads to its corresponding well-pronounced Debye-Scherrer diffraction rings in the selected area electron diffraction (SAED) pattern (see Fig. 2b) that can be assigned to the reflections (1 1 1), (2 0 0), (2 2 0), (3 1 1), (2 2 2), (4 0 0), (3 3 1) and (4 2 0) of cubic CeO_2. The ring pattern of the reflected planes from SAED corresponds to the fluorite structure of CeO_2, there are no additional rings in the SAED pattern stemming from any crystalline impurities.

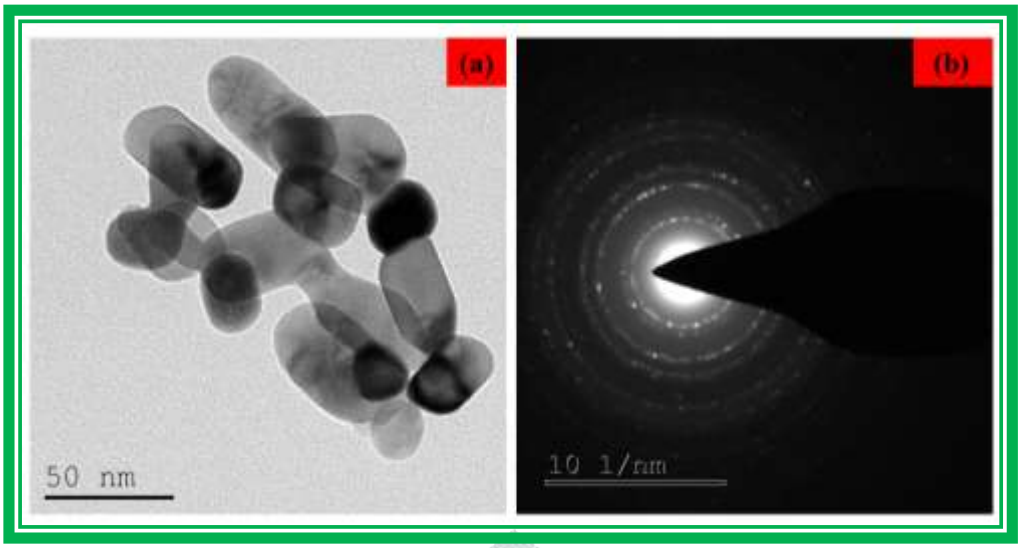

Figure 2(a-b) TEM images of CeO_2 NPs using *H. enneaspermus* leaf extract and (b) Selected Area Electron Diffraction.

3.3. Energy Dispersive Analysis X-Ray (EDAX) Spectra Studies

The compositional analysis of the CeO_2 NPs using *H. enneapermus* leaf extract was carried out using EDAX. The typical EDAX spectrum of the CeO_2 NPs is shown in **Fig. 3**. From the EDAX analysis, the *H. enneapermus* capped with CeO_2 NPs, the chemical compositions of C, Ce and O are found to be 12.90%, 25.57% and 61.53% respectively.

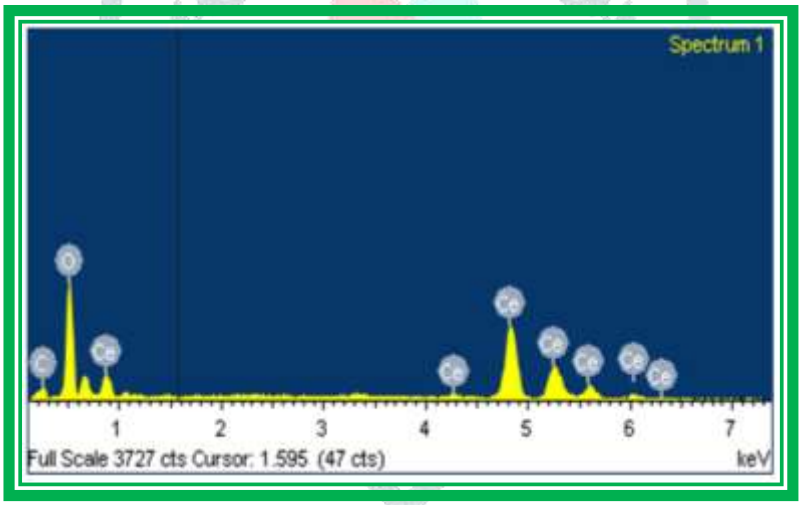

Figure 3 EDAX spectra of CeO_2 NPs using *H. enneaspermus* leaf extract.

3.4. Uv-Vis-Nir Spectroscopic Studies

The UV-VIS-NIR optical absorption spectra *H. enneaspermus* leaf extract assisted CeO_2 nanoparticles have been recorded in the range 190-1100nm is shown in Fig. 4a. From the absorption spectra, the absorption peaks are found at 321 nm for CeO_2 NPs, which can be attributed to the photo excitation of electron from valence band to conduction band.

The relation between the absorption coefficients α and the incident photon energy hυ can be written as

$$\alpha h\upsilon = A(h\upsilon - E_g)^n$$

Where E_g is the optical bandgap, A is the constant and the exponent n depends on the type of transition. The n = 1/2 for allowed direct transition, 2 for allowed indirect transition 3/2 and 3 for forbidden direct

and indirect transitions respectively. Considering direct band transition in without CeO_2 NPs, a plot between $(\alpha h\upsilon)^2$ vs. photon energy hυ and extrapolating the linear portion of the absorption edge to find the intercept with energy axis is shown in Fig. 4b. The estimated band gap of the CeO_2 sample is to be 2.9 eV. It can be seen that the CeO_2 sample shows an increase in Eg by a value exceeding 0.29, compared to the bulk CeO_2 powders (Eg = 3.19 eV, determined by UV-Visible spectroscopy) [20]. Thus there is a red shifting in the band gap of the material compared to bulk one. The red shifting occurs but it is expected that the red shifting is due to interfacial polaron effect arising from electron–phonon coupling and the coefficient of this coupling increases with decrease in size of semiconductor nanostructures [21]. Patsalas et al [22] have found that the red shift in the band gap is due to the presence of Ce^{3+} at grain boundaries and the gap decreases with the increase in [Ce^{3+}] concentration which forms some localized gap states in the band gap. Tatar et al [23] reported that the red shifting of band gap is due to the formation of some localized band gap states owing to oxygen vacancy and Ce^{3+}

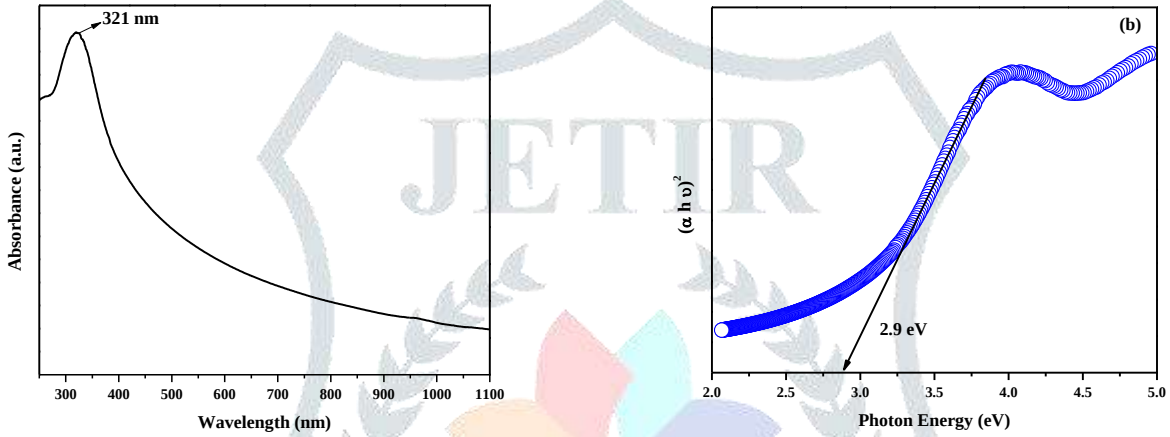

Figure 4 (a) UV-Visible spectrum of the phytosynthesized CeO_2 NPs. (b) Photon energy level of the phytosynthesized CeO_2 NPs

3.5. Fourier transform infra-red spectroscopy

The FT-IR spectra of CeO_2 NPs using *H. enneapermus* leaf extract is shown in **Fig. 5.** The broad absorption in the frequency band 3750-3000 cm^{-1} is assigned to O-H stretching from residual alcohols, water and Ce-OH. The absorption peak is observed at 3480 cm^{-1} for CeO_2 NPs. The CO_2 peaks are observed at 1389 cm^{-1} for CeO_2 NPs. These CO_2 band may arise due to some trapped CO_2 in air ambience. The band at 1608 cm^{-1} corresponds to the bending of H-O-H which is partly overlapping the O-C-O stretching band. Ce-O stretching is observed at 451 cm^{-1}[24, 17]. In our report, the Ce-O stretching band appeared in 457 cm^{-1}.

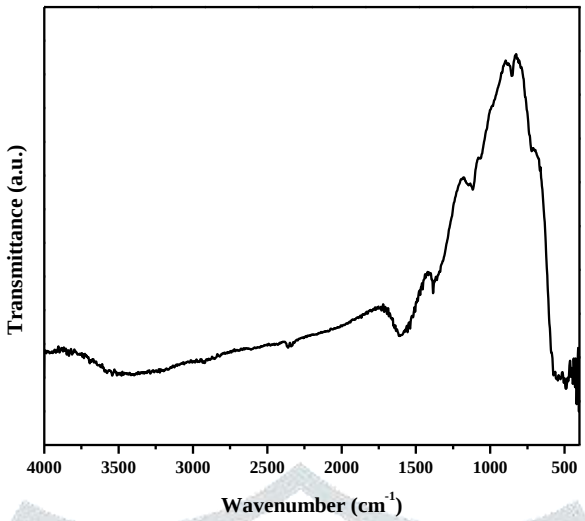

Figure 5 FTIR spectra of CeO_2 NPs using *H. enneaspermus* leaf extract

3.6. Photoluminescence (PL) studies.

The photoluminescence spectrum of the CeO_2 NPs using *H. enneaspermus* leaf extract is shown in **Fig. 6.** The photoluminescence spectra of the CeO_2 NPs using *H. enneaspermus* leaf extract samples recorded with the excited wavelength of 300 nm. The PL emission is observed for *H. enneaspermus* capped with CeO_2 samples covering from the very short wavelength of 340 nm to long wavelength 550 nm. A good fit of six peaks Gaussian function is obtained for all the PL spectra of the samples at the bottom labeled as M1, M2, M3, M4, M5 and M6. The solid lines represent the linear combination of six Gaussian peaks M1 has the lowest and M6 has the highest wavelength. The emission spectra of the *H. enneaspermus* leaf extract with CeO_2 NPs sample having six peaks at 366nm, 386nm, 418nm, 451nm, 482nm and 521nm. These bands are two Near Band Edge emission, Violet emission, blue emissions, blue-green emission and green emission respectively.

The NBE emissions M1 and M2 are located at UV region (366 and 386nm) for CeO_2 NPs. These NBE emissions are attributed to a band-to-band recombination process, possibly involving localized or free excitons [25]. The violet band M3 around 418 nm for the CeO_2 sample originates from the defect states existing extensively between the Ce 4f state and O 2p valence band [26]. These defects possibly act as radiative recombination centers for electron initially excited from the valence band to the 4f band of the CeO_2 [27]. The blue emission M4 at (451 nm) is related to the abundant defects such as dislocations, which is helpful for fast oxygen transportation. Ce 4f level with a width of 1 eV is localized at the forbidden gap, which lies at 3 eV over the valence band (O 2p). At room temperature, electron transition mainly occurs from defects level to O 2p level [28]. The blue-green emission M5 located at 482 nm is possibly due to surface defects in the CeO_2 NPs. The green emission M6 located at 521nm is attributed may be due to the low density of oxygen vacancies during the preparation of the CeO_2 sample.

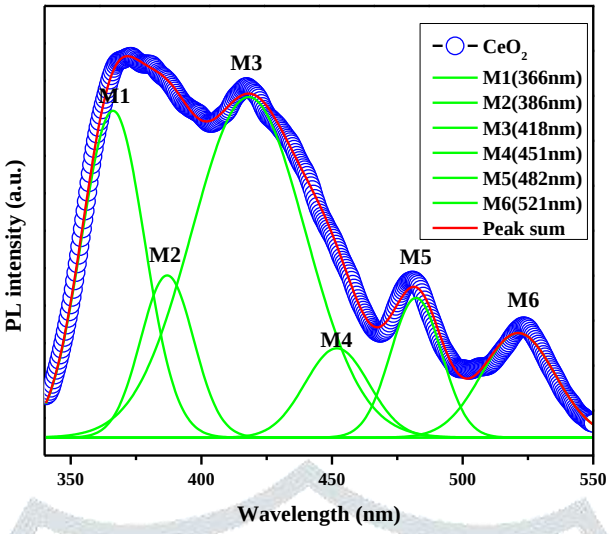

Figure 6 Photoluminescence emission spectra CeO_2 NPs using *H. enneaspermus* leaf extract

3.7. Cytotoxicity studies

The cytotoxic effect of the *H. enneaspermus* leaf extract with CeO_2 NPs is examined on cultured MCF- 7 human breast cancer cells by exposing cells for 24 h and 48 h to medium containing the CeO_2 NPs at 1-500 µg/ml concentration is shown in Fig. 7. In our results, that there is direct dose-response relationship with tested cells at higher concentrations. In relation to cell death, a minimum of 10 µg/ml of *H. enneaspermus* leaf extract capped with CeO_2 NPs is well enough to induce 50% of cell mortality. The CeO_2 NPs showed highly effective cytotoxic activity against MCF-7 cancer cells, and the IC_{50} value of the CeO_2 NPs is higher for 48 h treatment group than for 24 h treatment group. In fact, CeO_2 NPs may induce the reactive oxygen species. This CeO_2 NPs can lead to spontaneous ROS generation at their surface owing to their chemical and surface characteristics. They can also lead to the generation of free radicals after their interaction with cellular components, e.g., mitochondrial damage. Another way by which ROS is generated is through the activation of NADPH-oxidase enzyme which is responsible for O_2^- production in the membrane of phagocytic cells.

In case of CeO_2 NPs, the generation of ROS has been attributed to their semiconductor and nanolevel characteristic which leads to ROS generation even in the absence of light. These nanoparticles surface defects can lead to a large number of electron-hole pairs which can migrate to the nanoparticles surface and contribute to the ROS generation. The electrons and holes can react with the oxygen and hydroxyl ions, respectively, present in the aqueous environment of CeO_2 NPs. This produces highly reactive free radicals including the superoxide anion radical (from electrons) and the hydroxyl radical (from holes) [29]. When in contact with the cellular environment, these radicals can oxidize and reduce macromolecules (DNA, lipids, proteins) resulting in significant oxidative damage to cell [30]. Nevertheless, this is the first report on cytotoxic effects of green synthesized CeO_2 nanoparticles using *H. enneaspermus* plant extract against human Breast cancer (MCF-7) cell line.

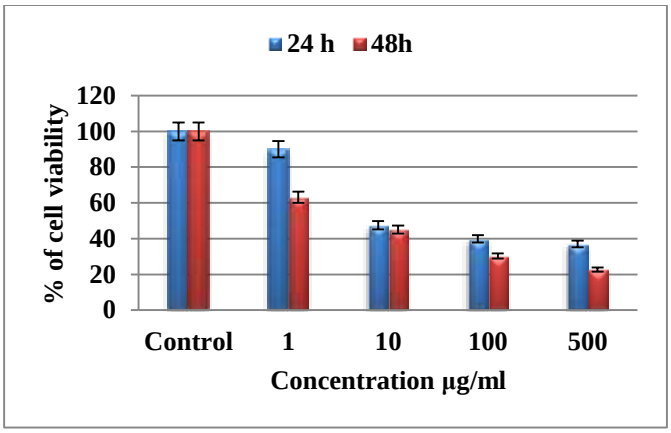

Figure 7 CeO_2 NPs using *H. enneaspermus* leaf extract concentration at 1-500 µg/ml.

3.8. Fluorescent Staining Method

The characteristic morphological changes are absorbed *H. enneaspermus* leaf extract capped with CeO_2 NPs is treated on cultured MCF- 7 human breast cancer cells have been evaluated by adopting fluorescent microscopic analysis of acridine orange/EthBr (AO/EB)-stained cells is shown in **Fig. 8(a-b)**. The results obtained reveal that the CeO_2 NPs induce cell death through different modes like apoptosis and necrosis. Upon treatment of the cells with IC_{50} concentration, apoptosis is a gene-controlled cell death process, which is characterized by DNA fragmentation, chromatin condensation and marginalization, membrane blebbing, cell shrinkage, and fragmentation of cells into membrane-enclosed vesicles or apoptotic bodies to be phagocytosed by macrophages [31]. The cytological changes observed are classified into four types according to the fluorescence emission and morphological features of chromatin condensation in the AO/EB-stained nuclei:(i) viable cells having uniformly green fluorescing nuclei with highly organized structure; (ii) early apoptotic cells (which still have intact membranes but have started undergoing DNA fragmentation) having green fluorescing nuclei but with perinuclear chromatin condensation visible as bright-green patches or fragments; (iii) late apoptotic cells having orange-to-red fluorescing nuclei with condensed or fragmented chromatin; (iv) necrotic cells, swollen to large sizes, having uniformly orange-to-red fluorescing nuclei with no indication of chromatin fragmentation. All of these morphological changes indicate that the cells are committed to death in such a way that both apoptotic and necrotic cells.

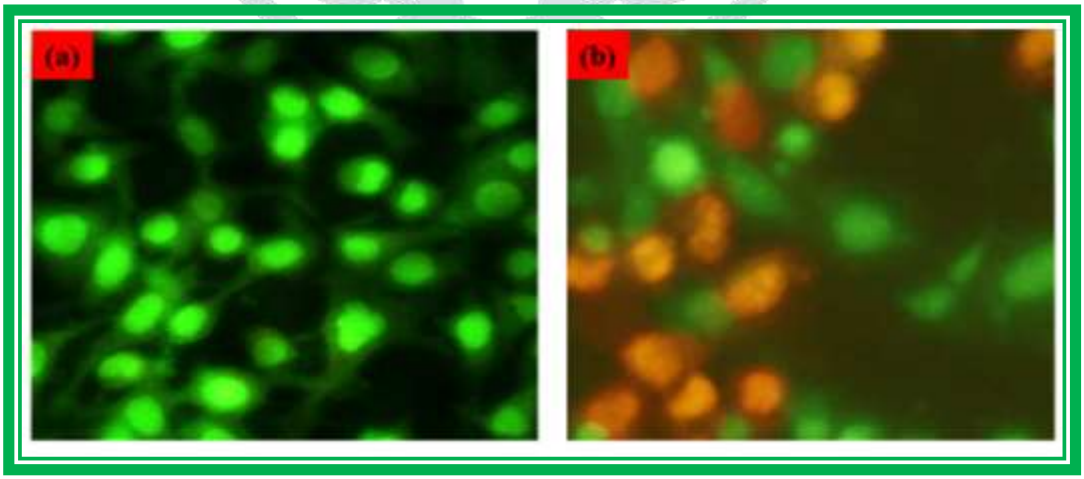

Figure 10: Morphological changes in the MCF-7 cells, reflecting apoptosis after exposure to CeO_2 NPs using *H. enneaspermus* leaf extract. Cells were treated with IC_{50} concentrations and morphological changes were observed using fluorescent microscope after staining with AO/EB. Photomicrographs of CeO_2 NPs treated cells show shrinkage of cells and fragmentation.

4. Conclusion

In summary, the synthesis of CeO_2 NPs using aqueous *H. enneaspermus* leaf extracts has been demonstrated. These CeO_2 NPs were prepared at ambient conditions with *H. enneaspermus* alkaloids acting as both the reducing and capping agents. The X-ray diffraction study confirmed that the prepared particles were of the cubic structure. From TEM images, the particle size is approximately 20-30 nm for spherical shape. From the EDAX analysis, the chemical compositions were estimated for the prepared CeO_2 samples. In FT-IR spectra, the various vibrational frequencies were assigned for the CeO_2 samples. From UV-Vis spectra, the *H. enneaspermus* capped CeO_2 samples absorption spectrum sharp peaks at 321 nm. The photoluminescence studies showed that the *H. enneaspermus* capped CeO_2 samples the band emission, which is due to oxygen vacancies and surface defects. The cytotoxic effect of the *H. enneaspermus* leaf extract capped with CeO_2 NPs was examined on cultured MCF- 7 human breast cancer cells by exposing cells for 24 hand 48 h. In vitro cytotoxic activity of green synthesized CeO_2 NPs against human breast cancer MCF-7 cell line was remarkable with 50% of mortality at 10µg/ml.

ACKNOWLEDGMENT

The authors wish to express their gratitude to the management of Jamal Mohamed College -620020, Tamil Nadu, India, for encouragement and providing necessary research facilities during this investigation.

References

[1] E. Bekyarova, P. Fornasiero, J. Kaspar, M. Graziani, Catal. Today 45 (1998) 179-183.
[2] S.B. Khan, M. Faisal, M.M. Rahman, A. Jamal, Sci. Total Environ. 409 (2011) 2987-2992.
[3] H. Yahiro, Y. Baba, K. Eguchi, A. Hiromichi, J. Electrochem. Soc. 135 (1998) 2077–2080.
[4] S. Yabe, T. Sato, J. Solid State Chem. 171 (2003) 7-11.
[5] S. Babu, J.H. Cho, J.M. Dowding, E. Heckert, C. Komanski, S. Soumen Das, J. Colon, C.H. Baker, M. Bass, W.T. Self, S. Seal, Chem. Commun. 46 (2010) 6915-6917.
[6] P. Zhang, Y. Ma, Z. Zhang, X. He, J. Zhang, Z. Guo, R. Tai, Y. Zhao, Z. Chai, ACS Nano, 11 (2012) 9943-9950.
[7] A. Thill, O. Zeyons, O. Spalla, F. Chauvat, J. Rose, M. Auffan, A.M. Flank, Environ. Sci. Technol. 40 (2006) 6151-6156.
[8] G. Sai Priya, A. Kanneganti, K. Anil Kumar, K. Venkateswara Rao, S. Bykkam, Internat. J. Sci. Res. Pub., 4 (2014) 1-4.
[9] K. R. Kirtikar, B. D. Basu, Indian Medicinal Plants, International Book Distributors. Dehradun, 1975, pp.212.
[10] R. Boominathan, B. Parimaladevi, S. C. Mandal, S, K. Ghoshal, J. Ethnopharmacol., 91, (2004), 367.
[11] R. Boominathan, B.P. Devi and S. C. Mandal, Phytotherapy Res., 17, (2003), 838.
[12] B. Weniger, L. Lagnika, C. Vonthron-Senecheau, D. Adjabimey, J. Gbenou, M. Moudachirou, R. Brun, R. Anton and A. J. Sanni, Ethnopharmacol., 90, (2004), 279.
[13] S. Hemlatha, A. K. Wahi, P. N. Singh, J. P. N. Chansouria., Indian J. Traditional Knowledg, 2 ,(2003), 389.
[14] D. K. Patel, R. Kumar , S. K. Prasad , K. Sairam, S. Hemalatha, Asian Pac J Trop Biomed. Aug 1(4), (2011), 316–322.
[15] S. Sahoo, D. M. Kar, S. Mohapatra1, S. P. Rout, S. K. Dash, 68 , (2006), 653-655.
[16] P. L. Majumdar, A. Basu, and D. Mal, Indian J. Chemistry, 17, (1979), 297.
[17] A. Arumugam, C. Karthikeyan, A.S.Haja Hameed , K.Gopinath , S. Gowri , V. Karthika, Mater. Sci. and Eng. C, 49 (2015) 408-415.
[18] M. Blagosklonny, W. S. El-Diery, Int. J. Cancer 67, (1996), 386.

[19]D.L. Spector, R.D. Goldman, L.A. Leinwand, Cell: A Laboratory Manual, Cultureand Biochemical Analysis of Cells, vol. 1, Cold Spring Harbor Laboratory Press, Cold Spring Harbor, New York, 1998, pp. 34.1-34.9.
[20] Z.Z. Orel, B. Orel, Phys. Status Solidi B 186 (1994) K33.
[21] C. Sun, H. Li, H. Zhang, Z. Wang, L. Chen, Nanotechnology 16 (2005) 1454.
[22] P. Patsalas, S. Logothetidis, L. Sygellou, S. Kennou, Phys. Rev. B 68 (2003) 035104.
[23] B. Tatar, E.D. Sam, K. Kutlu, M. Urgen, J. Mater. Sci. 43 (2008) 5102.
[24] E. K. Goharshadi, S. Samiee, P. Nancarrow, J. Colloid Interface Sci., 356 (2011) 473-480.
[25] L. Wang, J. Ren, X. Liu, G. Lu, Y. Wang, Mater. Chem. Phys. 127 (2011) 114–119.
[26] A.H. Morshed, M.E. Moussa, S.M. Bedair, R. Leonard, S.X. Liu, N.A. El-Masry, Appl. Phys. Lett. 70 (1997) 1647–1649.
[27] M.Y. Chen, X.T. Zu, X. Xiang, H.L. Zhang, Physica B 389 (2007) 263–268.
[28] C.L. Chai, S.Y. Yang, Z.K. Liu, M.Y. Liao, N.F. Chen, Chin. Sci. Bull. 48 (2003) 1198–1200.
[29] J. W Rasmussen, E. Martinez, P. Louka, D. G.Wingett, Expert Opin Drug Deliv., 7(9), (2010), 1063-1077.
[30] V. Sharma, D. Anderson, A. Dhawan, Apoptosis 17, (2012), 852-870.
[31] P.Moller, L.E.Knudsen, S.Loft, H.Wallin, Cancer Epidemiol. Biomarkers Prevent 9, (2000), 1005-1015.